Tumor Biol. (2015) 36:4467–4477
DOI 10.1007/s13277-015-3088-9

RESEARCH ARTICLE

Interpretation of immunohistochemistry data of tumor should consider microenvironmental factors

Huan Bian · Shuai Zhang · Huanhuan Wu · Yixiang Wang

Received: 21 October 2014 / Accepted: 8 January 2015 / Published online: 10 March 2015

Abstract The influence of tumor surrounding microenvironment is often neglected when immunohistochemistry is performed to investigate tumor properties and search biomarkers of cancer. This study was designed to evaluate whether the influence of tumor microenvironment on biological features of tumor cells should be taken into account for interpretation of the immunohistochemistry data of tumor specimens. In this study, we showed an example by using three tumor cell lines (HeLa, WSU-HN6, and Tca83) to establish tumor-caused bone destruction models in nude mice and then to investigate the influence of bone marrow microenvironment (BMM) on biological features of tumor cells. Immunohistochemistry results showed that, compared with tumor cells located outside of BMM, tumor cells located inside of BMM presented huge differences in the expression of inflammation-related proteins including tumor necrosis factor-α (TNF-α), TNF receptor-associated factor protein-6 (TRAF-6), phosphorylated-NF-κB p65 (p-p65), interleukin (IL)-6 and IL-11, matrix metalloproteinases including MMP-1, MMP-2, MMP-9, and MMP-13; and osteogenesis-related proteins including runt-related transcription factor 2 (RUNX2), bone sialoprotein (BSP), and osteocalcin (OCN) in all the models. However, when we compared the cell line pair derived from different sites (outside and inside of BMM, respectively) of the same HeLa tumor sample by real-time PCR, Western blot, and immunocytochemistry, the differences aforementioned in tumor tissues were not found. In addition, we verified that normal human bone marrow could not cause the above changes detected in vivo. Our results suggested that tumor-modified microenvironment could give the new biological features of the invaded tumor cells. Therefore, we should consider the influence of the surrounding microenvironment on tumor cells when we analyze tumor properties using immunohistochemistry.

Keywords Cancer microenvironment · Immunohistochemistry · Interpretation · Homologous cell lines

Introduction

Local invasion and distant metastasis can make tumor cells invade adjacent tissues or spread to distant tissues. Therefore, the tumor cells may have an opportunity to be affected by specific microenvironments such as the bone marrow microenvironment (BMM), brain and spinal marrow microenvironment and present different properties [1–5]. However, it is the fact that the influence of tumor microenvironment is often neglected when we use the immunohistochemistry to investigate the tumor properties and search a biomarker of tumor.

The aim of this study was to evaluate whether the effect of microenvironment on tumor properties should be taken into consideration when immunohistochemistry data are used to investigate tumor essential biological features. This is a very important question for making an accurate assessment and searching a biomarker of tumor. In this study, we used HeLa, WSU-HN6, and Tca83 tumor-caused bone destruction models to investigate the influence of BMM on the biological features of tumor cells. Through immunohistochemistry, we compared the tumor tissues located inside and outside of BMM in the

H. Bian · S. Zhang · H. Wu
Department of Oral and Maxillofacial Surgery, Peking University School and Hospital of Stomatology, 22 Zhongguancun Avenue South, Haidian District, Beijing 100081, China

Y. Wang (✉)
Central Laboratory, Peking University School and Hospital of Stomatology, 22 Zhongguancun Avenue South, Haidian District, Beijing 100081, China
e-mail: kqwangyx@sina.com

same specimens of the models. Then we generated a pair of homologous cell lines from tumor tissues located at different sites (outside and inside of the BMM, respectively) of the same HeLa tumor sample. Next, the homologous cell lines were compared with each other using real-time PCR, Western blot, and immunocytochemistry assays to explore whether the tumor features directly reflected by immunohistochemistry in the tumor specimens are intrinsic and heritable properties of the tumor or not. Finally, we investigated the influence of normal human bone marrow on the expression of detected genes and the mobility of WSU-HN6 cells in vitro by real-time PCR and wound healing assay. Our results demonstrated that the tumor microenvironment could affect the tumor biology properties tremendously and this should not be ignored when immunohistochemistry was used to investigate the intrinsic property of tumor.

Materials and methods

Cell culture

Human cervical carcinoma cell line HeLa, human head and neck squamous cell carcinoma cell line WSU-HN6, and human tongue squamous cell carcinoma cell line Tca83 were maintained in Dulbecco's Modified Eagle's Medium (DMEM; Gibco, Grand Island, NY, USA) or RPMI-1640 (Gibco), supplemented with 10 % fetal bovine serum (FBS; Gibco) and 1 % penicillin-streptomycin solution (Gibco) in a humidified incubator at 37 °C in an atmosphere of 5 % CO_2. Cells in mid-logarithmic growth (~75 % confluence) were used for the following experiments.

Establishment of tumor-caused bone destruction models in the lumbar vertebra and tibiae of nude mice

This study was approved by Medical Ethical Committee of the Peking University Health Center (LA2008-22). To confirm the data, we established two kinds of tumor-caused bone destruction models using HeLa, WSU-HN6, and Tca83 cells, which were injected into the erector spinae of the lumbar vertebra and tibiae of 6-week-old female BALB/c nude mice (3×10^6/mouse), respectively. At 30 days after tumor cell injection, the mice were sacrificed and the tumors with the invaded bone tissues were removed. All the tumor-caused spinal bone destruction samples and some tumor-caused tibia bone destruction specimens were fixed by 10 % formalin immediately. The fixed tumor-caused tibia bone destruction specimens were subjected to micro-CT analysis. The remaining fresh tumor samples were used to generate the paired homologous cell lines.

Micro-CT analysis of tumor-caused tibia bone destruction specimens

To detect the tumor-caused bone lesions in tibia destruction models, the fixed samples were scanned with micro-CT machine (Inveon MM CT; Siemens, USA).

Histological evaluation and immunohistochemistry

All the fixed tissue samples (tumor-caused spinal bone destruction samples and tumor-caused tibia bone destruction specimens) were decalcified in 17 % EDTA solution, embedded in paraffin wax, and sectioned into 4-μm slices for hematoxylin and eosin (HE) and immunohistochemistry staining. For immunohistochemistry, after dewaxing, the slides were dipped in 3 % hydrogen peroxide (H_2O_2) for 10 min to block endogenous peroxidase activity. After washing thrice in phosphate-buffered saline (PBS), antigen retrieval was performed with citrate buffer (0.01 M, pH 6.0) using microwave method or by incubating the slices with 1 % trypsin at 37 °C for 30 min depending on different demands of the primary antibodies. Then the slides were incubated with primary antibodies against pan-cytokeratin (pan-CK; used as supplied; Beijing Zhongshan Golden Bridge Biotechnology Co., Ltd., Beijing, China), tumor necrosis factor-α (TNF-α; 1:100 dilution; Santa Cruz Biotechnology, Inc., Santa Cruz, CA, USA), TNF receptor associated factor protein-6 (TRAF-6; 1:100; Santa Cruz Biotechnology), phosphorylated-NF-κB p65 (p-p65; 1:100; Santa Cruz Biotechnology), interleukin (IL)-6 (1:100; Santa Cruz Biotechnology), IL-11 (1:100; Santa Cruz Biotechnology), matrix metalloproteinase (MMP)-1 (1:100; Epitomics, Inc., CA, USA), MMP-2 (used as supplied; Beijing Zhongshan Golden Bridge Biotechnology Co., Ltd.), MMP-9 (used as supplied; Beijing Zhongshan Golden Bridge Biotechnology Co., Ltd.), MMP-13 (1:100; Epitomics), runt-related transcription factor 2 (RUNX2; 1:100; Santa Cruz Biotechnology), bone sialoprotein (BSP; 1:100; Santa Cruz Biotechnology), and osteocalcin (OCN; 1:100; Santa Cruz Biotechnology), respectively, in a humidified chamber at 4 °C overnight. After washing, the slides were treated with horseradish peroxidase (HRP)-conjugated secondary antibodies for 1 h at ambient temperature. The immunoreaction was detected using 3,3′-diaminobenzidine (DAB; Beijing Zhongshan Golden Bridge Biotechnology, Co., Ltd.) incubation for 1 min. Then the slides were counterstained with hematoxylin. Negative controls were performed using PBS instead of the primary antibodies. All slides were recorded using an Olympus DP controller (Olympus, Tokyo, Japan).

Analysis of immunohistochemistry images

Two investigators blinded to this study quantified the immunohistochemical staining of TRAF-6, p-p65, TNF-α, IL-6, IL-

11, MMP-1, MMP-2, MMP-9, MMP-13, RUNX2, BSP, and OCN in the tumor cells located outside and inside of the BMM. Ten random high-power fields (×400 magnification) of immunohistochemistry images were selected for each sample to do further analysis. Mean optical density (integrated optical density/area) of positive reactions of the tumor cells in each image was analyzed with Image-Pro Plus 6.0 (Media Cybernetics, Bethesda, MD, USA) after color segmentation with the fixed threshold value of hue, saturation, and intensity (HSI) [6–8].

Generation of HeLa-TOB and HeLa-TIB cell lines from tumor-caused bone destruction models in the tibiae of nude mice

After being removed from the bodies of nude mice, some HeLa-caused tibia bone destruction specimens were used immediately to generate homologous cell lines from the same HeLa tumor tissue. One cell line was derived from the tumor tissue located outside of the BMM and the other was derived from the tumor tissue located inside of the BMM, hereafter named as HeLa-TOB cell line and HeLa-TIB cell line, respectively. The procedure of tissue culture was performed carefully. For generation of HeLa-TOB cell line, a small soft tumor tissue which was far away from the BMM was removed from the HeLa tumor sample and cut into about 1-mm^3 tissue blocks. For the HeLa-TIB cell line generation, the remaining soft tissue outside of the tibia BMM was entirely removed by shearing, scraping, and washing. In order to further eliminate the tumor cells outside of the BMM, the bare tibia was digested by 0.25 % Trypsin-EDTA at 37 °C for 5 min and washed three times with PBS. Then the tibia was cut into small fragments (1 mm^3) with new surgical instruments. After that, the two kinds of small tissue blocks mentioned above were cultured in T25 flasks separately with DMEM containing 10 % FBS and 1 % penicillin-streptomycin solution at 37 °C in a humidified 5 % CO_2 atmosphere. About 1–2 weeks after tissue culture, single colony-derived cell lines were found, isolated, and expanded, and then identified by immunocytochemistry staining for pan-CK, a biomarker for cells of epithelial origin.

Real-time PCR

Tumor cells in mid-logarithmic growth were used for real-time PCR. Total RNA was extracted from the tumor cells using TRIzol reagent (Invitrogen, Carlsbad, CA, USA), and cDNA was obtained by reverse transcription with the GoScript™ Reverse Transcription System (Promega, Madison, WI, USA). Relative quantitative real-time PCR reactions were performed with SYBR Green PCR master mix (Roche, Indianapolis, IN, USA) in an ABI Prism 7000 Sequence Detection System (Applied Biosystems, Life Technologies, Warrington, UK). GAPDH was used as the endogenous control. The primers of each target gene are listed in Table 1. The thermal cycling consisted of 10 min at 95 °C, followed by 40 cycles at 95 °C for 15 s, and at 60 °C for 1 min. All amplifications were performed in triplicate for each sample and repeated three times independently. Relative expression of the target genes was analyzed using the $2^{-\Delta\Delta Ct}$ method.

Western blot

HeLa-TOB and HeLa-TIB cells in mid-logarithmic growth were used for Western blot. After washing with ice PBS, the tumor cells were lysed on ice in RIPA buffer (Applygen Technologies, Inc. Beijing, China) supplemented with protease inhibitors (Roche). The concentration of total protein was determined using BCA protein assay kit (Thermo Fisher Scientific Inc., Rockford, USA). Equal quantities of protein (25 μg) were separated by sodium dodecyl sulfate-polyacrylamide gel electrophoresis (SDS-PAGE; Applygen Technology) and transferred to polyvinylidene difluoride membranes (Millipore Corporation, Billerica, MA, USA). The membranes were blocked in 5 % nonfat dry milk for 1 h and probed

Table 1 The sequences of real-time PCR primers used in this study

Gene	Forward primers (5′–3′)	Reverse primers (5′–3′)
GAPDH	ATGGGGAAGGTGAAGGTCG	GGGGTCATTGATGGCAACAATA
TRAF-6	CCCTACAGCCCCAATTCCAT	GCGTGCCAAGTGATTCCTCT
TNF-α	GTGCTTGTTCCTCAGCCTCT	GCTTGTCACTCGGGGTTCGA
IL-6	GTGAGGAACAAGCCAGAGC	TACATTTGCCGAAGAGCC
MMP-1	TCTGGGGTGTGGTGTCTCA	GCCTCCCATCATTCTTCAGGTT
MMP-2	GCCCCAGACAGGTGATCTTG	GCTTGCGAGGGAAGAAGTTGT
MMP-9	GCCCGACCCGAGCTGACTC	TTCAGGGCGAGGACCATAGAGG
MMP-13	TTTCAACGGACCCATACAGTTTG	CATGACGCGAACAATACGGTTA
RUNX2	TCCTATGACCAGTCTTACCCCT	GGCTCTTCTTACTGAGAGTGGAA
BSP	GAACCTCGTGGGGACAATTAC	CATCATAGCCATCGTAGCCTTG
OCN	CACTCCTCGCCCTATTGGC	CCCTCCTGCTTGGACACAAAG

with primary antibodies against p-p65 (1:1000; Epitomics), total-p65 (t-p65;1:1000; Cell Signaling Technology, Inc., Danvers, MA, USA), IL-6 (1:500; Epitomics), MMP-1 (1:1000; Epitomics), MMP-2 (1:300; Santa Cruz Biotechnology), MMP-9 (1:1000; Cell Signaling Technology), MMP-13 (1:1000; Epitomics), RUNX2 (1:300; Santa Cruz Biotechnology), BSP (1:300; Santa Cruz Biotechnology), and GAPDH (1:1000; Beijing Zhongshan Golden Bridge Biotechnology Co., Ltd.), respectively, at 4 °C overnight. After incubation with HRP-linked secondary antibodies, the protein bands were visualized using an enhanced chemiluminescent substrate (Applygen Technology).

Immunocytochemistry

HeLa-TOB and HeLa-TIB cells in mid-logarithmic growth were used for immunocytochemistry. Briefly, tumor cells (1×10^4 cells per well) were plated onto the sterile glass slides in 24-well plates and grown for 48 h. After that, they were fixed with 95 % ethanol, permeabilized with 0.1 % Triton X-100, treated with 3 % H_2O_2, blocked in 5 % horse serum, and incubated with the same primary antibodies as used in immunohistochemistry overnight at 4 °C. After washing with PBS, the slides were treated with HRP-conjugated secondary antibodies for 1 h at room temperature and incubated with DAB to perform the color development and counterstained with hematoxylin. Negative controls were prepared with omission of the primary antibodies. All glass slides were observed under a microscope, and images were recorded using an Olympus DP controller (Olympus).

Preparation of diluted bone marrow from a healthy donor and investigation of its influences on WSU-HN6 cells through real-time PCR and wound healing assays

Bone marrow was obtained from the posterior superior iliac spine of a 45-year-old healthy woman who underwent bone marrow donation in Peking University First Hospital with informed consent. The bone marrow was centrifuged with $400\times g$ for 30 min to remove red blood cells, then suspension was filtered through a 70-μm filter and stored in −20 °C freezer. The bone marrow diluted with DMEM at 1:10 ratio (BM-CM) was used to treat WSU-HN6 cells for real-time PCR and wound healing assays.

Wound healing assay

WSU-HN6 cells were plated in six-well-plates and cultured as confluent monolayer. Then the cell monolayer was treated with mitomycin (30 μg/mL) for 2 h and scratched using a sterile 200-μl pipette tip. The scratched cells were removed by washing with PBS for three times. After that, the cell monolayer was cultured with serum-free DMEM or BM-CM. The wound areas were photographed at 0 and 12 h after scratch with a microscope (TE-2000U; Nikon, Tokyo, Japan). The scratch width at different time points was measured, and finally the relative migration speed was calculated.

Statistical analysis

All experiments were repeated at least three times. Data were presented as means±standard deviation (SD).

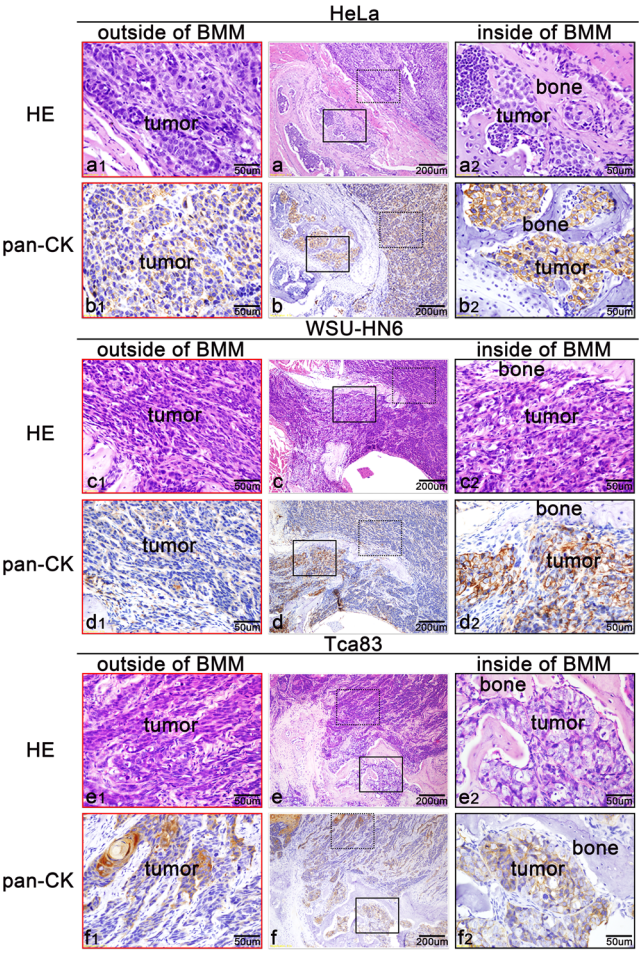

Fig. 1 HE stain and immunohistochemistry staining for pan-cytokeratin (pan-CK) of the HeLa-, WSU-HN6-, and Tca83-caused spinal bone destruction samples. The *middle column* represented the original low magnification (×100) images (*a*, *b*, *c*, *d*, *e*, and *f*), in which *black dotted bordered rectangles* represented tumor tissues located outside of BMM, and *black line rectangles* represented tumor tissues located inside of BMM. The images of the *left column* (*a1*, *b1*, *c1*, *d1*, *e1*, and *f1*) represented the magnification fields of *black dotted bordered rectangles* in the corresponding original figures, while the images of the *right column* (*a2*, *b2*, *c2*, *d2*, *e2*, and *f2*) represented the magnification fields of *black line rectangles* in the corresponding original figures. In these images, bone destruction lesions have been induced by the three cancer cell lines, and pan-CK immunohistochemistry results further confirmed the neoplasms located outside and inside of BMM are epithelial original cells. In addition, the morphology of TOB and TIB cells was different. Compared with TOB cells, TIB cells presented much larger with plentiful cytoplasm and lightly stained vesicular nucleus in the three tumor-caused bone destruction models. The *left*, *middle*, and *right columns*, as well as *black dotted bordered* and *black line rectangles* represented the same meaning in following figures

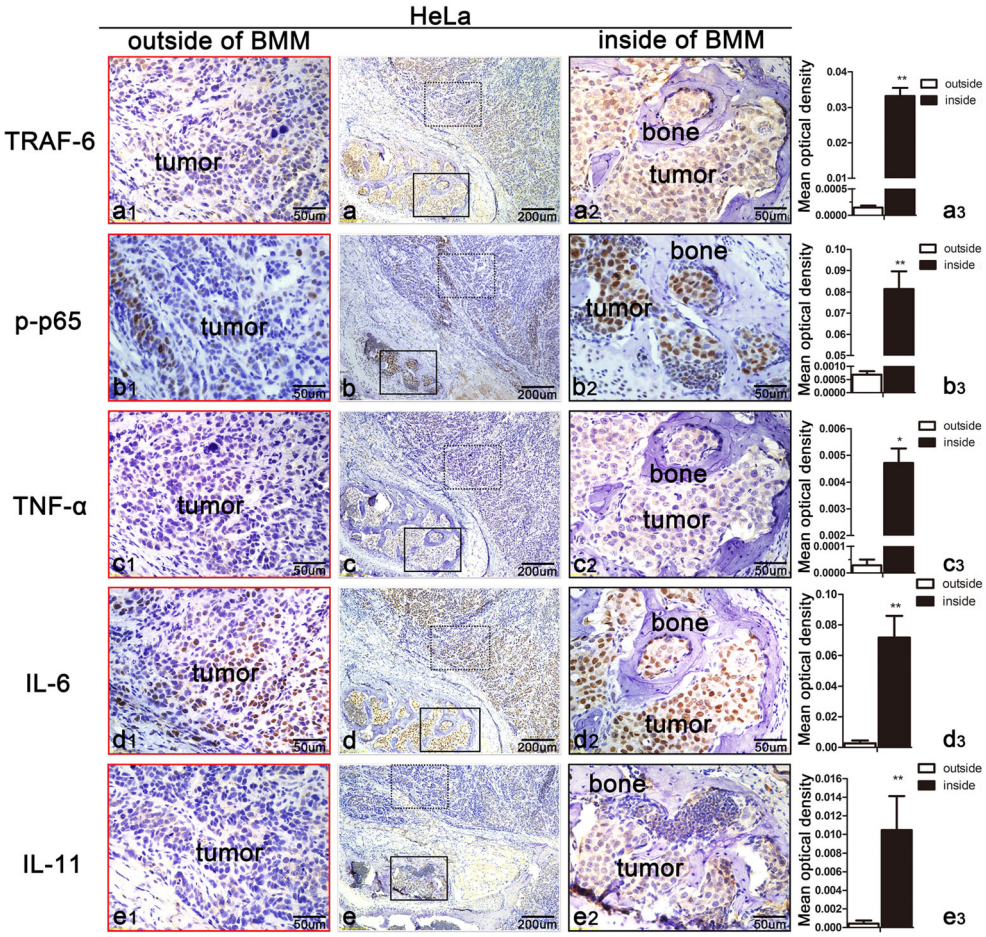

Fig. 2 Expression pattern of inflammation-related molecules in HeLa-caused spinal bone destruction samples. The results showed that TIB cells were strongly positive to inflammation-related molecules TRAF-6, p-p65, TNF-α, IL-6, and IL-11 compared with TOB cells. *$P<0.05$; **$P<0.01$

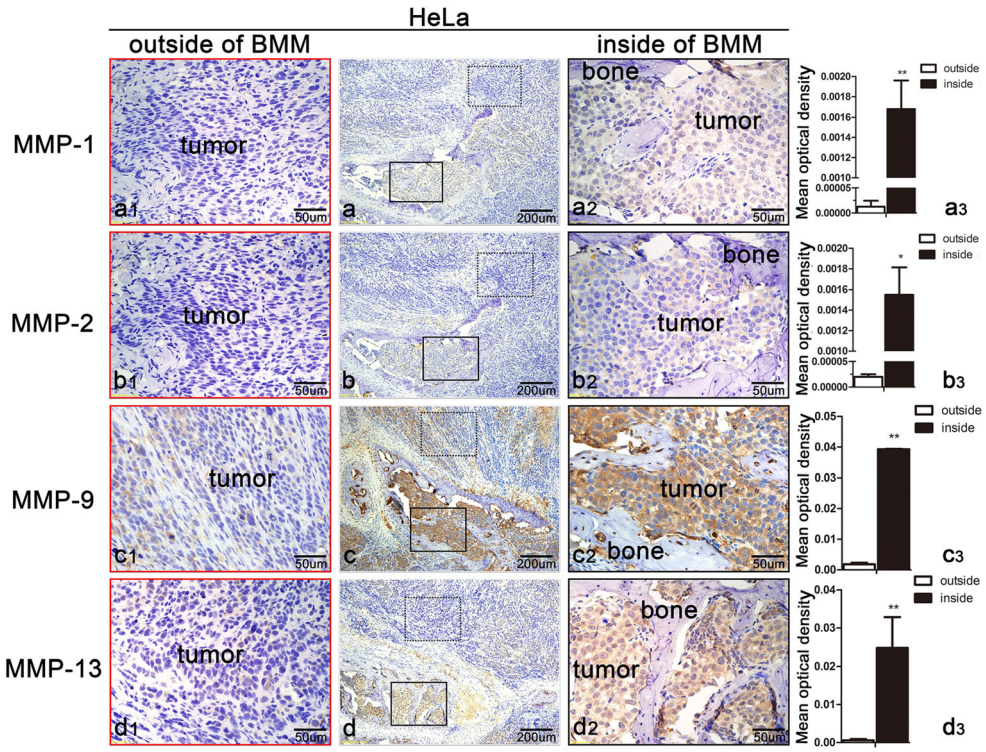

Fig. 3 Expression pattern of MMPs in HeLa-caused destructive bone lesions in the lumbar vertebra of nude mice. The results showed that TIB cells were much more positive to MMP-1, MMP-2, MMP-9, and MMP-13 than TOB cells. *$P<0.05$; **$P<0.01$

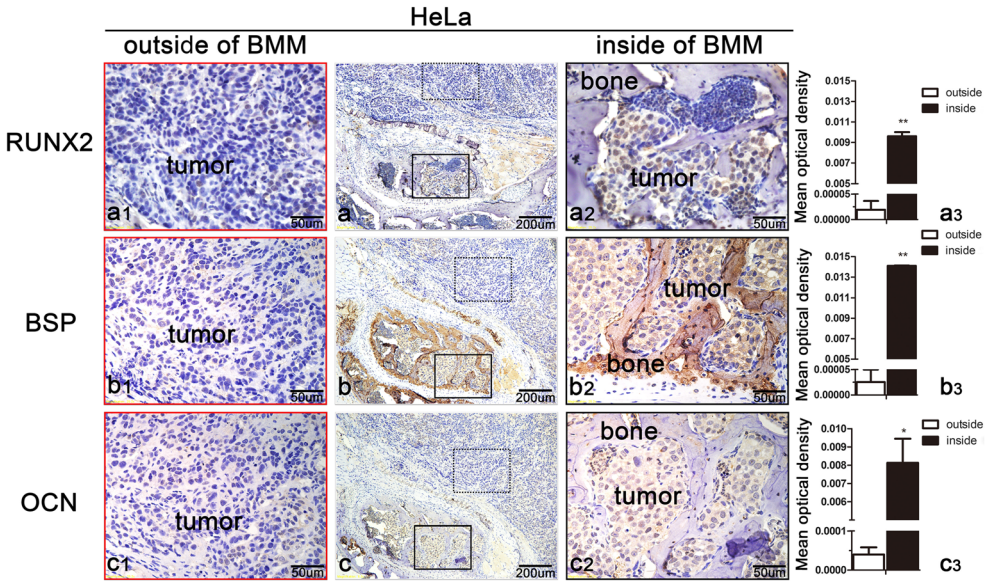

Fig. 4 Expression pattern of osteogenesis-related genes in HeLa-caused spinal bone destruction specimens. The results showed that TIB cells were much more positive to RUNX2, BSP, and OCN than TOB cells. *$P<0.05$; **$P<0.01$

Statistical analyses were performed by independent sample *t*-test with SPSS 13.0 software (SPSS Inc., Chicago, IL, USA). *P* value <0.05 was defined as significant difference.

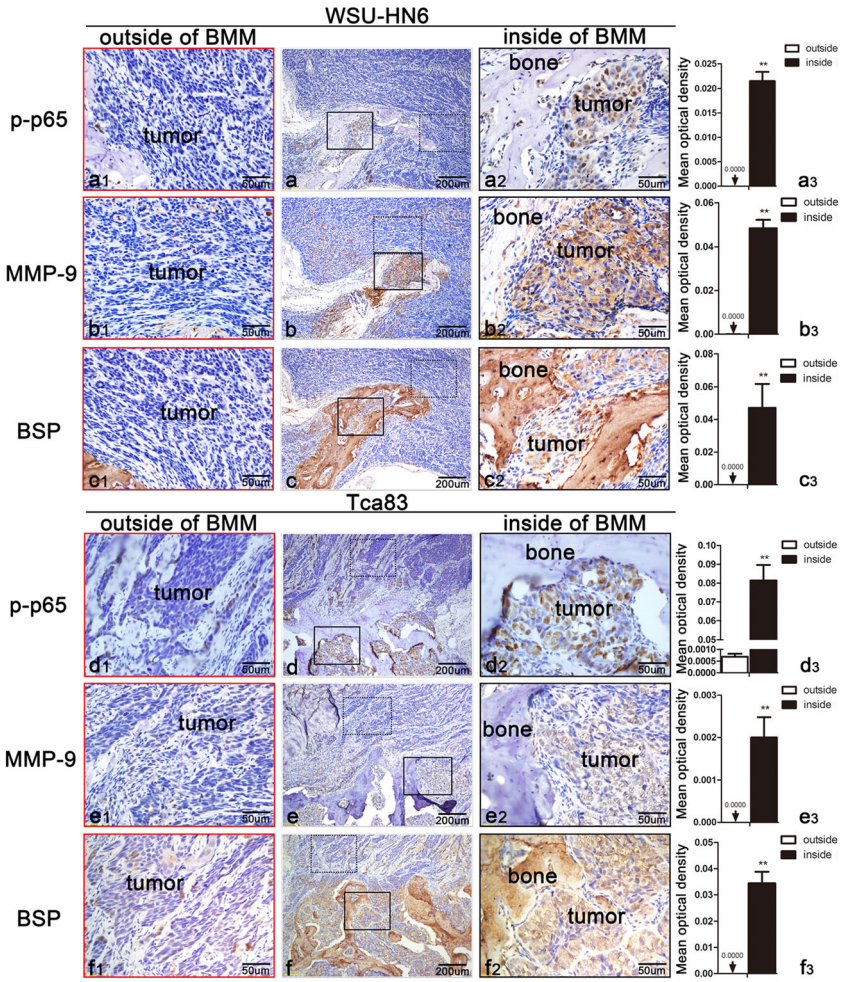

Fig. 5 Expression pattern of p-p65, MMP-9, and BSP in WSU-HN6- and Tca83-caused destructive bone lesions in the lumbar vertebra of nude mice. The results showed that in WSU-HN6 and Tca83 samples, p-p65, MMP-9, and BSP present the same expression pattern as those in HeLa-caused spinal bone destruction specimens. TIB cells were strongly positive to p-p65, MMP-9, and BSP compared with TOB cells. *$P<0.05$; **$P<0.01$

Results

Tumor-caused destructive bone lesions in the lumbar vertebra of BALB/c nude mice

HE stain and immunohistochemistry for pan-CK showed that HeLa, WSU-HN6, and Tca83 tumor cells invaded into the BMM in tumor-induced spinal bone destruction models (Fig. 1). In high magnification fields (×400) of HE stain, we found a different morphology between tumor cells located outside of BMM (TOB cells) and tumor cells located inside of BMM (TIB cells). Compared with TOB cells, TIB cells were much larger with plentiful cytoplasm and lightly stained vesicular nucleus. The immunohistochemistry for pan-CK clearly showed that tumor cells located both outside and inside of BMM were positive for pan-CK, a classical epithelial cell biomarker [9], which further confirmed that the invaded cells were tumor cells.

Tumor cells located inside of BMM (TIB cells) presented different biological features with tumor cells located outside of BMM (TOB cells)

The expression of some specific molecules which play a significant role during tumor progression was investigated by immunohistochemistry in tumor-caused spinal bone destruction samples. These molecules included (1) inflammation-related molecules including TRAF-6, p-p65, TNF-α, IL-6, and IL-11 which can promote the progression of tumor cells in bone and induce osteoclast differentiation [10–13], (2) MMPs including MMP-1, 2, 9, and 13 which exerted an important role in invasion and metastasis of tumor through degradation of the extracellular matrix (ECM) [14–16]; and (3) osteogenesis-related molecules including RUNX2, BSP, and OCN which were traditionally thought to be specifically expressed in bone and recently had been ectopically detected in a number of cancers (such as breast cancer and prostate cancer) and were significantly associated with the

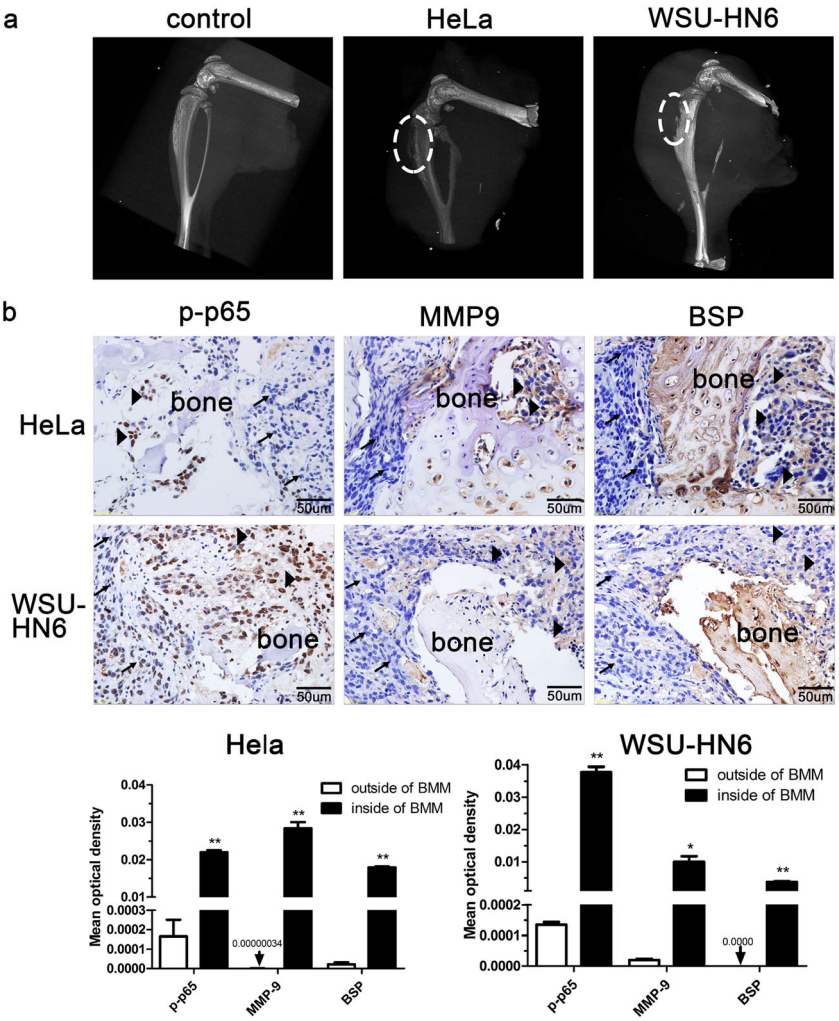

Fig. 6 Micro-CT analysis and immunohistochemistry of HeLa- and WSU-HN6-caused bone destruction models in the tibia of nude mice. **a** Micro-CT results showed that HeLa and WSU-HN6 tumor cells clearly caused decreased bone mineral density and interruption of bone continuity (indicated by the *dotted ovals*). **b** Immunohistochemistry results showed that TIB cells (indicated by *black triangles*) were strongly positive to p-p65, MMP-9, and BSP compared with TOB cells (indicated by *black arrows*) in these two tumor cell-caused tibia bone destruction models. The images of the immunohistochemistry were obtained at×400 magnification. **P*<0.05; ***P*<0.01

development of bone metastases and poor prognosis [17–25]. In HeLa-caused spinal bone destruction samples, the results showed that compared with TOB cells, TIB cells presented (1) higher levels (higher mean optical density values of the positive reactions) of TRAF-6 (P=0.000), p-p65 (P=0.003), TNF-α (P=0.018), IL-6 (P=0.003), and IL-11 (P=0.009) (Fig. 2); (2) higher levels of MMP-1 (P=0.009), MMP-2 (P=0.017), MMP-9 (P=0.000), and MMP-13 (P=0.007) (Fig. 3); and (3) higher levels of RUNX2 (P=0.000), BSP (P=0.000), and OCN (P=0.012) (Fig. 4). In WSU-HN6- and Tca83-caused spinal bone destruction samples, the results showed the similar expression patterns as those in HeLa samples. Here, we only showed are the results and statistical P values of p-P65 (P=0.000 for WSU-HN6 samples, P=0.020 for Tca83 samples), MMP-9 (P=0.002 for WSU-HN6 samples, P=0.002 for Tca83 samples), and BSP (P=0.005 for WSU-HN6 samples, P=0.005 for Tca83 samples) (Fig. 5).

Micro-CT analysis and immunohistochemistry of tumor-caused bone destruction models in the tibia of nude mice

The micro-CT results clearly showed that both HeLa and WSU-HN6 tumor cells caused reduction in bone mineral density and interruption of bone continuity in the affected tibiae after 1-month inoculation of tumor cells (Fig. 6a). Immunohistochemistry for TRAF-6, p-p65, TNF-α, IL-6, IL-11, MMP-1, MMP-2, MMP-9, MMP-13, RUNX2, BSP, and OCN were also performed to investigate the biological features of tumors in these samples. The results showed that TIB cells expressed higher levels of TRAF-6, p-p65, TNF-α, IL-6, IL-11, MMP-1, MMP-2, MMP-9, MMP-13, RUNX2, BSP, and OCN than TOB cells, which were similar with those obtained in tumor-caused spinal bone destruction samples. Here, showed only are part of the results (Fig. 6b).

In vitro studies showed the paired TOB-TIB cell lines did not present the same biological features detected in in vivo studies

HeLa-TOB cell line and its paired cell line HeLa-TIB cell line were successfully generated from the corresponding tissues as described in the "Materials and methods" section (Fig. 7a). The HeLa-TOB and HeLa-TIB cells in mid-logarithmic growth were subjected to real-time PCR, Western blot, and immunocytochemistry. Real-time PCR results showed that all the detected genes including IL-6, TNF-α, MMP-1, MMP-2, MMP-9, MMP-13, RUNX2, and OCN were equally expressed at mRNA level in HeLa-TOB cells and HeLa-TIB cells (Fig. 7b). Western blot showed that HeLa-TOB cells and HeLa-TIB cells equally expressed p-p65, t-p65, IL-6, MMP-1, MMP-2, MMP-9, MMP-13, RUNX2, and BSP at protein level (Fig. 7c). Immunocytochemistry further showed that the HeLa-TOB cells and HeLa-TIB cells expressed same levels of

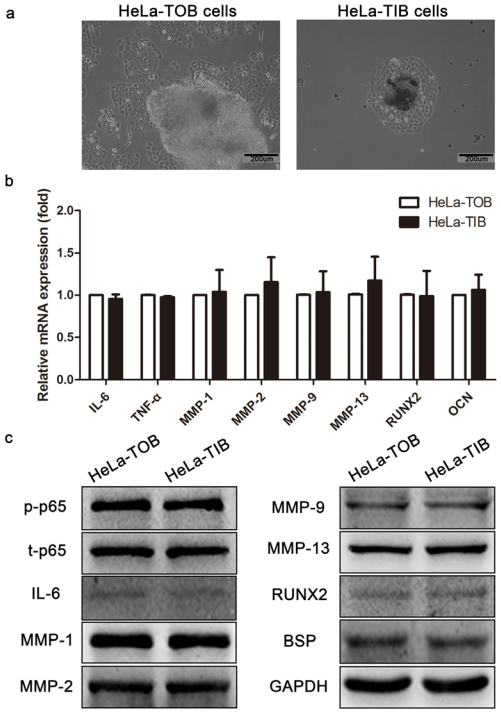

Fig. 7 Generation of HeLa-TOB and HeLa-TIB cell line pair and screening of the specific molecules expression with real-time PCR and Western blot. **a** HeLa-TOB and HeLa-TIB cell lines were generated successfully. **b** Real-time PCR and **c** Western blot results showed that the detected genes were equally expressed at mRNA and protein levels in HeLa-TOB and HeLa-TIB cells

TRAF-6, p-p65, TNF-α, IL-6, IL-11, MMP-1, MMP-2, MMP-9, MMP-13, RUNX2, BSP, and OCN in vitro (Fig. 8).

Influences of BM-CM on expression of the indicated targets and mobility of WSU-HN6 in vitro

Real-time PCR results showed that at 24-h posttreatment, the BM-CM could upregulate the expression of TNF-α, IL-6, and MMP-9; downregulate TRAF-6, MMP-1, MMP-2, MMP-13, BSP, and OCN expression; and could not affect RUNX2 expression in WSU-HN6 cells (Fig. 9a). Wound healing assay result showed that the BM-CM could not affect the mobility of WSU-HN6 cells (Fig. 9b). These results indicated that the BM derived from healthy people played a totally different role when compared with tumor-modified bone marrow.

Discussion

Immunohistochemistry has been widely used in clinic and basic research since the early 1940s [9, 26]. At present, immunohistochemistry is considered an important laboratory examination method for doctors and researchers because it can provide evidence to diagnose, classify, and determine the

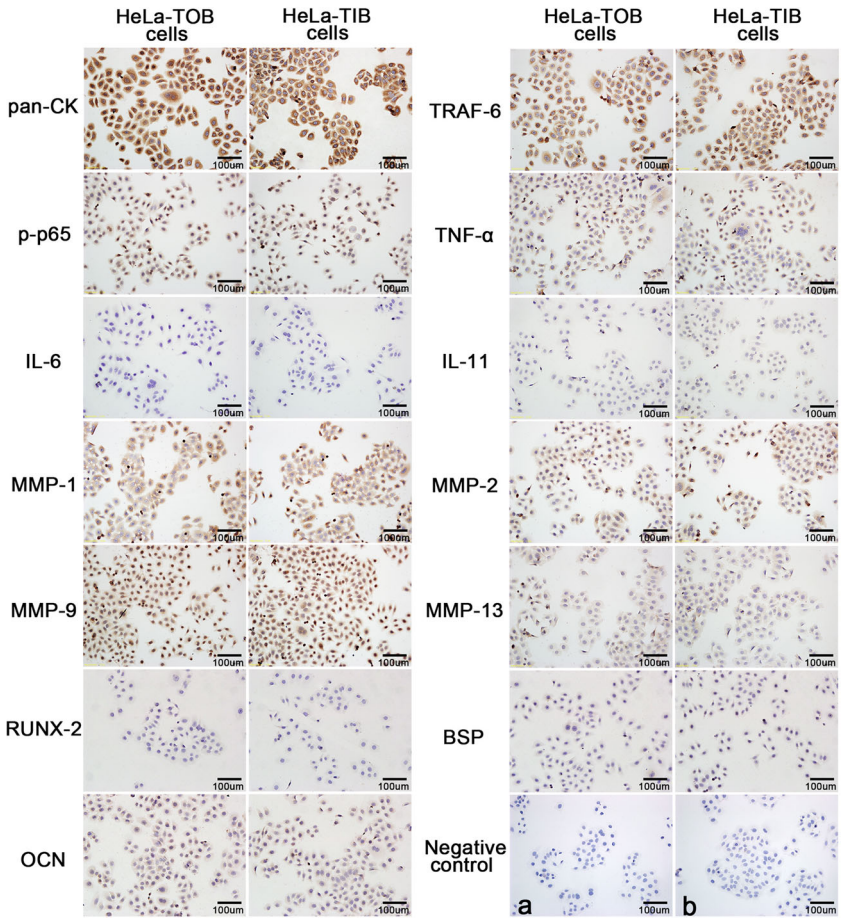

Fig. 8 Immunocytochemistry for specific molecules of HeLa-TOB and HeLa-TIB cells. The results showed there was no obvious difference between HeLa-TOB and HeLa-TIB cell lines. **a**, **b** Negative controls that used anti-rabbit HRP-conjugated secondary antibody and anti-mouse HRP-conjugated secondary antibody, respectively

prognosis of primary and metastatic tumors [27–29]. Because of this point, it is necessary to pay more attention to the evaluation of immunohistochemistry data in order to avoid any bias conclusion.

It is well known that the different organs separate with each other in the body and contain differently specific microenvironments. They do have some distinct environment in the human body, for example, BMM, brain and spinal marrow microenvironment, and these places are common sites of tumor metastasis. Once tumor cells enter into different microenvironments through invasion and metastasis, they may present specific phenotype owing to microenvironmental stimulation. Normally, we consider the environment factor in cancer initiation and development. The term "field cancerization" is used to describe an area of epithelium preconditioned by unknown processes, finally predisposed towards the development of cancer [30–33]. It emphasizes the role of microenvironment on the initiation and progression of tumor [33]. However, when we use immunohistochemistry to explore the tumor essential property and investigate the biomarker of cancer in tumor specimens, especially in tiny clinical tumor samples, the effect of microenvironment is usually neglected. We tend to attribute all the properties reflected by the immunohistochemistry directly to the nature of tumor and neglect that some presented properties are not cancer essential features, but given by tumor surrounding microenvironment, thus maybe leading to an inaccurate conclusion.

In this study, we used three tumor cell lines to establish two types of tumor-induced bone destruction models and investigated the influence of BMM on the biological features of tumor cells. Our HE and immunohistochemistry data of tumor samples clearly showed that TIB cells were obviously distinct from TOB cells not only in morphology but also in some important biological features, which indicated the tremendous influence of BMM on the features of tumor cells. However, when we compared HeLa-TOB cell line with HeLa-TIB cell line through real-time PCR, Western blot, and immunocytochemistry, there was no markedly difference found as had been found in tumor samples by immunohistochemistry. These results mean that the TOB cells and TIB cells are same in intrinsic and the different properties detected by immunohistochemistry were caused by the different surrounding microenvironments and did not represent the intrinsic differences between TOB cells and TIB cells.

Given that the tumor immunophenotypes were markedly changed by tumor-modified BMM, the question is raised that whether the normal bone marrow can alter the immunophenotypes and mobility of tumor cells in vitro. Therefore, we obtained the

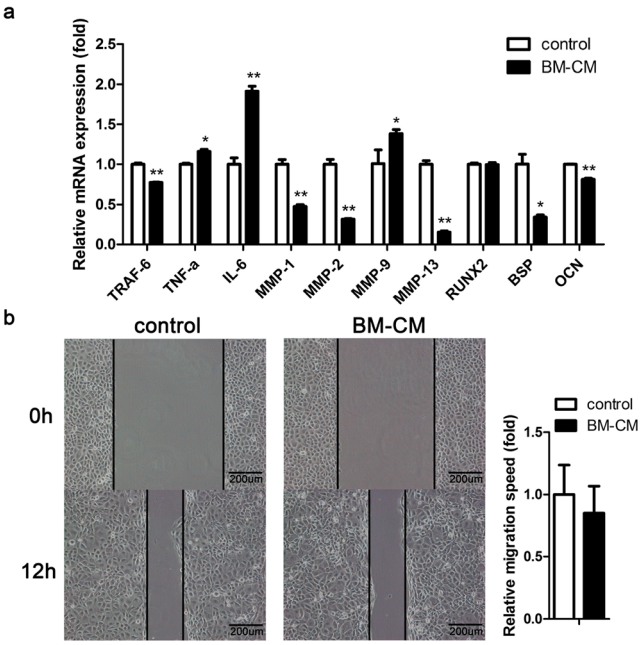

Fig. 9 Influences of BM-CM on WSU-HN6 cells. **a** Real-time PCR results showed that after 24 h treatment with BM-CM the WSU-HN6 cells expressed higher levels of TNF-α, IL-6, and MMP-9; lower levels of TRAF-6, MMP-1, MMP-2, MMP-13, BSP, and OCN; and equal level of RUNX2 at mRNA levels compared with control group. **b** Wound healing assay showed that the BM-CM could not affect the mobility of WSU-HN6 cells. *$P<0.05$; **$P<0.01$

normal bone marrow from a healthy donor and used the cell-removed BM-CM to treat WSU-HN6 cells. Surprisingly, the real-time PCR results showed that most of the examined molecules including TRAF-6, MMP-1, MMP-2, MMP-13, BSP, and OCN were significantly downregulated by BM-CM except TNF-α, IL-6, MMP-9, and RUNX2. These results were different from the immunohistochemistry data of tumor samples. Furthermore, the wound healing assay result showed that BM-CM treatment could not affect the mobility of WSU-HN6 cells, which indicated that the bone marrow derived from healthy people played almost a totally different role when compared with tumor-modified BMM. Our explanations are (1) normal bone marrow can keep the balance between osteogenesis and osteoclastogenesis and maintain the homeostasis of bone marrow [13, 34]. (2) Once tumor cells invade the specific microenvironment, the homeostasis of both bone and bone marrow will be destroyed [34, 35]. Plenty of bioactive molecules embedded in the bone tissue will be released into the bone marrow when the bone is destructed [13, 34]. (3) Meanwhile, tumor cells, as well as tumor-associated host cells, can secrete numerous cytokines. The newly formed BMM is a tumor-modified BMM rather than the intrinsic microenvironment, which gives the acquired biological features of the invaded tumor cells.

In fact, microenvironment has been mentioned in the studies regarding tumor hypoxia [36–38]. Tumor outgrows its blood supply, thus yields hypoxic environment in the inner of tumor tissue, which finally leading to alteration of metabolism [39] as well as the corresponding biological features of cancer cells [40–42]. So when tumor tissue comes from a small tumor and tumor tissue comes from a big tumor were compared with immunohistochemistry, if different properties were found, we should deliberate that the differences can reflect the intrinsic differences of the tumors or just caused by the different microenvironments (such as non-hypoxic and hypoxic microenvironments).

The main aim of studying tumor biology is to look for the characteristics of tumor in nature, so as to accurately diagnose and effectively manage the tumor. Obviously, if the conclusion we got were based on the immunohistochemistry data described above, although the data are true, we may only get the noise, which makes us far away from the truth of tumor in essence. From this point of view, to accurately reflect the characteristics of cancer, the microenvironment surrounding the lesions should be taken into consideration in immunohistochemistry analysis in the future, especially for samples originated from the significantly different microenvironment. Only in this way can we approach to the intrinsic property of tumor and effectively manage the disease in the future.

In conclusion, our results suggest that tumor-modified microenvironment can significantly alter the biological features of tumor, which cannot be ignored in evaluating immunohistochemistry results of tissue specimens.

Acknowledgments The work was supported by the research grants from Special Fund for Development of Capital Health care (2011-4025-02), Nature Science Foundation of Heilongjiang Province, China (Grant No. QC2014C107), and the Ministry of Science and Technology of China under contract International Science & Technology Cooperation Program Foundation (Grant No. 1019).

Conflicts of interest None

References

1. Ordonez-Moran P, Huelsken J. Complex metastatic niches: already a target for therapy? Curr Opin Cell Biol. 2014;31C:29–38.
2. Erin N, Kale S, Tanriover G, Koksoy S, Duymus O, Korcum AF. Differential characteristics of heart, liver, and brain metastatic subsets of murine breast carcinoma. Breast Cancer Res Treat. 2013;139:677–89.
3. Wood SL, Pernemalm M, Crosbie PA, Whetton AD. The role of the tumor-microenvironment in lung cancer-metastasis and its relationship to potential therapeutic targets. Cancer Treat Rev. 2014;40:558–66.
4. Rahim F, Hajizamani S, Mortaz E, Ahmadzadeh A, Shahjahani M, Shahrabi S, et al. Molecular regulation of bone marrow metastasis in prostate and breast cancer. Bone Marrow Res. 2014;2014:405920.
5. Rondeau G, Abedinpour P, Desai P, Baron VT, Borgstrom P, Welsh J. Effects of different tissue microenvironments on gene expression in breast cancer cells. PLoS One. 2014;9:e101160.

6. Shi H, Hayes M, Kirana C, Miller R, Keating J, Macartney-Coxson D, et al. TUFM is a potential new prognostic indicator for colorectal carcinoma. Pathology. 2012;44:506–12.
7. Pei J, Fu W, Yang L, Zhang Z, Liu Y. Oxidative stress is involved in the pathogenesis of Keshan disease (an endemic dilated cardiomyopathy) in China. Oxid Med Cell Longev. 2013;2013:474203.
8. Cong L, Pu CQ, Shi Q, Wang Q, Lu XH. Complement membrane attack complex is related with immune-mediated necrotizing myopathy. Int J Clin Exp Pathol. 2014;7:4143–9.
9. Labelle P, Reilly CM, Naydan DK, Labelle AL. Immunohistochemical characteristics of normal canine eyes. Vet Pathol. 2012;49:860–9.
10. Zhu LJ, Dai L, Zheng DH, Mo YQ, Ou-Yang X, Wei XN, et al. Upregulation of tumor necrosis factor receptor-associated factor 6 correlated with synovitis severity in rheumatoid arthritis. Arthritis Res Ther. 2012;14:R133.
11. Furuta H, Osawa K, Shin M, Ishikawa A, Matsuo K, Khan M, et al. Selective inhibition of NF-kappaB suppresses bone invasion by oral squamous cell carcinoma in vivo. Int J Cancer. 2012;131:E625–35.
12. Tang CH, Chuang JY, Fong YC, Maa MC, Way TD, Hung CH. Bone-derived SDF-1 stimulates IL-6 release via CXCR4, ERK and NF-kappaB pathways and promotes osteoclastogenesis in human oral cancer cells. Carcinogenesis. 2008;29:1483–92.
13. Chen YC, Sosnoski DM, Mastro AM. Breast cancer metastasis to the bone: mechanisms of bone loss. Breast Cancer Res. 2010;12:215.
14. 14 Bodnar M, Szylberg L, Kazmierczak W, Marszalek A. Tumor progression driven by pathways activating matrix metalloproteinases and their inhibitors. J Oral Pathol Med 2014.
15. Chakravarthi BV, Pathi SS, Goswami MT, Cieslik M, Zheng H, Nallasivam S, et al. The miR-124-Prolyl Hydroxylase P4HA1-MMP1 axis plays a critical role in prostate cancer progression. Oncotarget. 2014;5:6654–69.
16. Balbin M, Pendas AM, Uria JA, Jimenez MG, Freije JP, Lopez-Otin C. Expression and regulation of collagenase-3 (MMP-13) in human malignant tumors. Apmis. 1999;107:45–53.
17. McDonald L, Ferrari N, Terry A, Bell M, Mohammed ZM, Orange C, et al. RUNX2 correlates with subtype-specific breast cancer in a human tissue microarray, and ectopic expression of Runx2 perturbs differentiation in the mouse mammary gland. Dis Model Mech. 2014;7:525–34.
18. Baniwal SK, Khalid O, Gabet Y, Shah RR, Purcell DJ, Mav D, et al. Runx2 transcriptome of prostate cancer cells: Insights into invasiveness and bone metastasis. Mol Cancer. 2010;9:258.
19. Pratap J, Lian JB, Javed A, Barnes GL, van Wijnen AJ, Stein JL, et al. Regulatory roles of Runx2 in metastatic tumor and cancer cell interactions with bone. Cancer Metastasis Rev. 2006;25:589–600.
20. Zhang JH, Wang J, Tang J, Barnett B, Dickson J, Hahsimoto N, et al. Bone sialoprotein promotes bone metastasis of a non-bone-seeking clone of human breast cancer cells. Anticancer Res. 2004;24:1361–8.
21. Waltregny D, Bellahcene A, de Leval X, Florkin B, Weidle U, Castronovo V. Increased expression of bone sialoprotein in bone metastases compared with visceral metastases in human breast and prostate cancers. J Bone Miner Res. 2000;15:834–43.
22. Ogbureke KU, Nikitakis NG, Warburton G, Ord RA, Sauk JJ, Waller JL, et al. Up-regulation of SIBLING proteins and correlation with cognate MMP expression in oral cancer. Oral Oncol. 2007;43:920–32.
23. Salem AM, Zohny SF, Abd EM, Hamdy R. Predictive value of osteocalcin and beta-CrossLaps in metastatic breast cancer. Clin Biochem. 2007;40:1201–8.
24. Gardner TA, Lee SJ, Lee SD, Li X, Shirakawa T, Kwon DD, et al. Differential expression of osteocalcin during the metastatic progression of prostate cancer. Oncol Rep. 2009;21:903–8.
25. Huang WC, Xie Z, Konaka H, Sodek J, Zhau HE, Chung LW. Human osteocalcin and bone sialoprotein mediating osteomimicry of prostate cancer cells: role of cAMP-dependent protein kinase a signaling pathway. Cancer Res. 2005;65:2303–13.
26. Moskaluk CA, Baras AS, Mancuso SA, Fan H, Davidson RJ, Dirks DC, et al. Development and characterization of xenograft model systems for adenoid cystic carcinoma. Lab Invest. 2011;91:1480–90.
27. Krishna M. Diagnosis of metastatic neoplasms: an immunohistochemical approach. Arch Pathol Lab Med. 2010;134:207–15.
28. Pu Y, Wang L, Wu H, Feng Z, Wang Y, Guo C. High MMP-21 expression in metastatic lymph nodes predicts unfavorable overall survival for oral squamous cell carcinoma patients with lymphatic metastasis. Oncol Rep. 2014;31:2644–50.
29. Sakashita T, Homma A, Suzuki S, Hatakeyama H, Kano S, Mizumachi T, et al. Prognostic value of cyclin D1 expression in tumor-free surgical margins in head and neck squamous cell carcinomas. Acta Otolaryngol. 2013;133:984–91.
30. Liao CT, Wallace CG, Lee LY, Hsueh C, Lin CY, Fan KH, et al. Clinical evidence of field cancerization in patients with oral cavity cancer in a betel quid chewing area. Oral Oncol. 2014;50:721–31.
31. Luo Y, Yu M, Grady WM. Field cancerization in the colon: a role for aberrant DNA methylation? Gastroenterol Rep (Oxf). 2014;2:16–20.
32. Torezan LA, Festa-Neto C. Cutaneous field cancerization: clinical, histopathological and therapeutic aspects. An Bras Dermatol. 2013;88:775–86.
33. 33 Lochhead P, Chan AT, Nishihara R, Fuchs CS, Beck AH, Giovannucci E, Ogino S. Etiologic field effect: reappraisal of the field effect concept in cancer predisposition and progression. Mod Pathol 2014.
34. Roodman GD. Mechanisms of bone metastasis. N Engl J Med. 2004;350:1655–64.
35. Thomas RJ, Guise TA, Yin JJ, Elliott J, Horwood NJ, Martin TJ, et al. Breast cancer cells interact with osteoblasts to support osteoclast formation. Endocrinology. 1999;140:4451–8.
36. Ackerman D, Simon MC. Hypoxia, lipids, and cancer: surviving the harsh tumor microenvironment. Trends Cell Biol. 2014;24:472–8.
37. Ji RC. Hypoxia and lymphangiogenesis in tumor microenvironment and metastasis. Cancer Lett. 2014;346:6–16.
38. Spivak-Kroizman TR, Hostetter G, Posner R, Aziz M, Hu C, Demeure MJ, et al. Hypoxia triggers hedgehog-mediated tumor-stromal interactions in pancreatic cancer. Cancer Res. 2013;73:3235–47.
39. Zeng W, Liu P, Pan W, Singh SR, Wei Y. Hypoxia and hypoxia inducible factors in tumor metabolism. Cancer Lett 2014
40. Hasmim M, Messai Y, Noman MZ. Chouaib S [Tumor hypoxia: a key player in the regulation of stromal and anti-tumor responses]. Med Sci (Paris). 2014;30:422–8.
41. Tsai YP, Wu KJ. Hypoxia-regulated target genes implicated in tumor metastasis. J Biomed Sci. 2012;19:102.
42. Ren Y, Hao P, Dutta B, Cheow ES, Sim KH, Gan CS, et al. Hypoxia modulates A431 cellular pathways association to tumor radioresistance and enhanced migration revealed by comprehensive proteomic and functional studies. Mol Cell Proteomics. 2013;12:485–98.